



Contents lists available at ScienceDirect

Arabian Journal of Chemistry

journal homepage: www.sciencedirect.com



# Solvent-free synthesis of jasminaldehyde over chitosan-layered double hydroxide catalyst assisted by microwave irradiation

Jamal Houssaini<sup>a,\*</sup>, Mohammed Naciri Bennani<sup>a</sup>, Said Arhzaf<sup>a</sup>, Chadia Mounir<sup>a</sup>, Marwa Alaqrbeh<sup>b</sup>, Hammou Ahlafi<sup>a</sup>, Abdellatif Amhoud<sup>c</sup>

<sup>a</sup>Laboratory of Chemistry and Biology Applied to the Environment, URL-CNRST N°13, Research Team "Materials and Applied Catalysis", Chemistry Department, Faculty of Sciences, Moulay Ismail University, BP. 11201 Zitoune, Meknes 50000, Morocco

<sup>b</sup>Prince Al Hussein bin Abdullah II Academy for Civil Protection, Al-Balqa Applied University, Al-Salt 19117, Jordan

<sup>c</sup>Laboratory of Materials, Membranes and Nanotechnology, Department of Chemistry, Faculty of Sciences, Moulay Ismail University, BP. 11201 Zitoune, Meknes 50000, Morocco

## ARTICLE INFO

### Article history:

Received 18 July 2023

Accepted 1 October 2023

Available online 6 October 2023

### Keywords:

Chitosan

Layered double hydroxide

Microwave irradiation

Catalytic activity

Aldol condensation

Jasminaldehyde

## ABSTRACT

This research paper reports on the use of chitosan-modified layered double hydroxide (LDH) composite catalysts (CS/MgAl-NO<sub>3</sub>) for the synthesis of jasminaldehyde under microwave irradiation. The catalysts were prepared by co-precipitation in an inert nitrogen atmosphere. The resulting samples were characterized by mean of X-ray diffraction (XRD), Fourier transform infrared spectroscopy (FT-IR), thermogravimetric/differential thermal analysis (TGA/DTA), scanning electron microscope (SEM) with energy-dispersive X-ray (EDX), and N<sub>2</sub> adsorption/desorption isotherm (BET) analysis. The basicity of each catalyst was determined by the acid-base titration method. The performance of the catalysts was evaluated in the solvent-free synthesis of jasminaldehyde from aldol by condensation reaction between benzaldehyde and 1-heptanal in a microwave oven at P = 100 W and T = 90 °C. The effects of different parameters that are involved in the reaction, such as the catalyst amount and the benzaldehyde to 1-heptanal molar ratio, and reaction temperature, are investigated in detail. The results showed that the CS-functionalization of the catalyst leads to the enhancement of its basic sites making it more efficient than the naked MgAl-NO<sub>3</sub> catalyst, in terms of the initial reaction rate, the conversion of the reactants and the selectivity toward the jasminaldehyde. The CS/MgAl-NO<sub>3</sub> catalyst was also evaluated in successive regeneration reaction cycles.

© 2023 Published by Elsevier B.V. on behalf of King Saud University. This is an open access article under the CC BY-NC-ND license (<http://creativecommons.org/licenses/by-nc-nd/4.0/>).

## 1. Introduction

In synthetic organic chemistry, water has always been preferred by researchers as a solvent over organic solvents, in order to develop a green environmental pathway in organic synthesis, without harmful waste. For example, water plays an important role in aqueous organocatalytic aldol condensation reactions, for the construction of new C-C bonds. Especially, the aldol condensation reaction, which is performed on different catalysts between alde-

hydes or aldehydes and ketones (Zheng et al., 2018), has long been used in organic chemistry for building a variety of carbon-carbon bonds. Because it allows the production of a variety of organic compounds, which have extensive industrial applications (Alzhrani et al., 2019). Among these, jasminaldehyde which is also known as  $\alpha$ -amylcinnam-aldehyde is widely used in industries such as cosmetics and perfumes (Pratap, 2022). Apart from its natural source, it can be synthesized via the aldol condensation of benzaldehyde and 1-heptanal with liquid bases such as sodium hydroxide or potassium hydroxide, and this process has been intensively studied by researchers to enhance the yield of jasminaldehyde (Sharma et al., 2010). However, the presence of liquid bases in the reaction medium generates undesirable by-products, contributing to environmental pollution. To overcome this inconvenience, several solid base heterogeneous catalysts have been developed in recent years, and used in basic synthetic chemistry (Debecker et al., 2009; Othman et al., 2009; Tampieri et al., 2020), due to their basic properties, the ability for their reuse

\* Corresponding author.

E-mail address: [jamal.houssaini@edu.umi.ac.ma](mailto:jamal.houssaini@edu.umi.ac.ma) (J. Houssaini).

Peer review under responsibility of King Saud University.



and the ease of their separation from the reaction medium (Wang & Ohare, 2012). It was shown that the higher reaction rate is achieved using basic catalysts, instead of acid catalysts. In addition, several parameters, which are involved in the reaction of aldol condensation, were examined in order to obtain the higher selectivity to jasminaldehyde, (Chen et al., 2015; Ganga et al., 2016; Hajek et al., 2015; Sharma et al., 2008). For example, Wong et al. conducted a study on a nanocrystalline base aluminosilicate F-type zeolite catalyst, which was prepared using rice husk ash as a silica source (Wong et al., 2018), found that the microwave irradiation enhanced the conversion of aldol condensation reaction of 1-heptanal with benzaldehyde to jasminaldehyde up to 77.1%. Z. Gholami et al. indicated that both Bronsted and Lewis ( $O^{2-}$ ) basic sites and Lewis acid sites on the surface of the Mg–Al catalyst, improve the catalytic activity and selectivity in synthesis of jasminaldehyde over Mg–Al catalyst derived from hydrotalcite-like precursors (Gholami et al., 2020). Hamza & Nagaraju, also concluded that the high performance of amorphous metal aluminophosphate catalysts in terms of catalytic activity (76%) and selectivity (71%) to jasminaldehyde, is due to the cooperative role of the optimal amount of acidic and basic sites (Hamza & Nagaraju, 2015). On the other hand, magnesium oxide was found to be inadequate catalyst for the synthesis of jasminaldehyde because of its monobasic properties, while the bifunctional  $MgO-NO_3-H_2O_2$  acid-base catalyst leads to high conversion (99%) and selectivity (88%) to jasminaldehyde after 5.5 h of reaction at 140 °C (Gholami et al., 2020). This was explained by the fact that the bifunctional catalyst favored the adsorption of benzaldehyde over 1-heptanal. According to literature data (Fan, 2020; Ganga et al., 2016; Pagadala et al., 2014; Varma, 2001), it seems that the conversion and the selectivity of the used catalysts to produce jasminaldehyde from benzaldehyde and heptanal condensation depend on various parameters, among which the initial molar ratio of the reactants (B/H)<sub>0</sub> and the number of basic/acid adsorption sites on the catalysts. However, the synthesis of jasminaldehyde, using particularly the CS/LDH type catalyst has not been investigated in the aldol condensation. In addition, most of the previous studies, focused on the study of a single experimental parameter effect on the performance of the catalysts employed. Thus, the development of efficient catalysts and the selection of the appropriate experimental conditions would lead to a very high conversion and selectivity to jasminaldehyde. Therefore, attention to this aspect is of great importance and is worth to be further explored. This constitutes the aim of the present work where the catalytic performance of new elaborated bimetallic layered double hydroxide, MgAl–NO<sub>3</sub>, and CS/MgAl–NO<sub>3</sub> composite catalysts, with the Mg/Al ratio of 3, were investigated in the synthesis of jasminaldehyde from aldol condensation reaction between benzaldehyde and 1-heptanal (Scheme 1). The reaction was made in the absence of solvent and under microwave irradiation. The latter was chosen because it was proven to be a highly effective heating method in some reactions due to its ability to achieve favorable conversion rates in

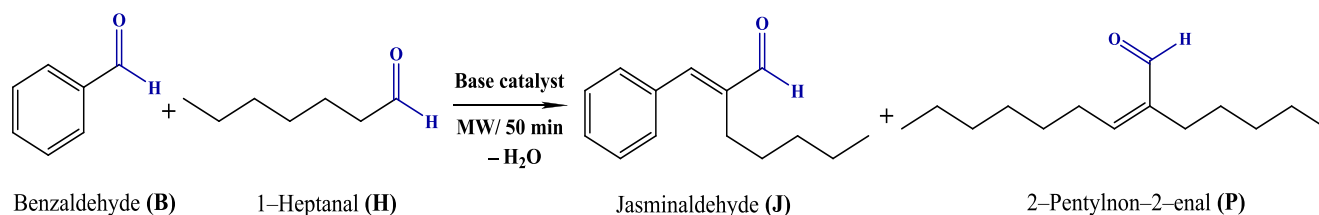
shorter reaction time, compared with conventional heating methods (Narasimharao et al., 2013) to prevent a large amount of liquid waste in the reaction medium (Rana & Rana, 2014; Varma, 2001).

Layered double hydroxide is a two-dimensional ionic clay material with a structure similar to hydrotalcite. It consists of layers of cationic metal and anionic interlayer regions, allowing for ion exchange (Abd El-Monaem et al., 2023). Their structure is similar to that of brucite  $Mg(OH)_2$ , in which part of the  $Mg^{2+}$  cations, coordinated octahedrally by hydroxyl ions, are replaced by  $Al^{3+}$  ions forming positively charged layers. These positive charges are balanced by the presence of hydrated interlayer anions. The general formula for LDH is  $[M_{1-x}^{2+} M_x^{3+} (OH)_2]^{x+} [A_{x/n}^{n-} mH_2O]^{x-}$ , where  $M^{2+}$  and  $M^{3+}$  refer to divalent and trivalent metal cations, respectively. Examples of divalent metal cations include  $Mg^{2+}$ ,  $Zn^{2+}$ ,  $Ni^{2+}$ ,  $Fe^{2+}$ ,  $Mn^{2+}$ , and others, while trivalent metal cations include  $Al^{3+}$ ,  $Fe^{3+}$ ,  $Co^{3+}$ ,  $Cr^{3+}$ , and others.  $A^{n-}$  denotes exchangeable anions present between the layers, such as  $CO_3^{2-}$ ,  $NO_3^-$ ,  $Cl^-$ , and similar anions. By varying the nature and proportions of cations and anions, different compounds can be synthesized using this formula (Bernard et al., 2022; Mokhtar et al., 2021). LDH have notable chemical and physical properties and are easily fabricated at a low cost. The combination of different  $M^{2+}$  and  $M^{3+}$  metals in LDH makes them efficient heterogeneous catalysts for various applications including catalysis, cosmetics, and adsorption (Eltaweil et al., 2023). Additionally, the use of the natural biopolymer CS, which correspond to a linear polysaccharide of  $\beta$ -(1,4)-linked glucosamine units (2-amino-2-deoxy- $\beta$ -D-glucopyranose) (Scheme 2), presents additional advantages due to its lower cost, biocompatibility, biodegradability, non-toxicity and insolubility in water (Molnár, 2019). It has good thermal and chemical stability and a large number of hydroxyl (–OH) and primary amino (–NH<sub>2</sub>) groups. On the other hand, CS combined with transition metals has been employed as a heterogeneous catalyst for various reactions (Abdelkrim, 2015; Serhan et al., 2019). Furthermore, the functionalization of LDH with CS biopolymer can improve the properties of LDH-based-catalysts due to the additional sites of CS, such as the functional basic amino and hydroxyl groups (Alghamdi et al., 2019; Chatterjee et al., 2019; Serhan et al., 2019). Before their use, the physicochemical properties of all samples prepared by the coprecipitation method were characterized using different characterization techniques.

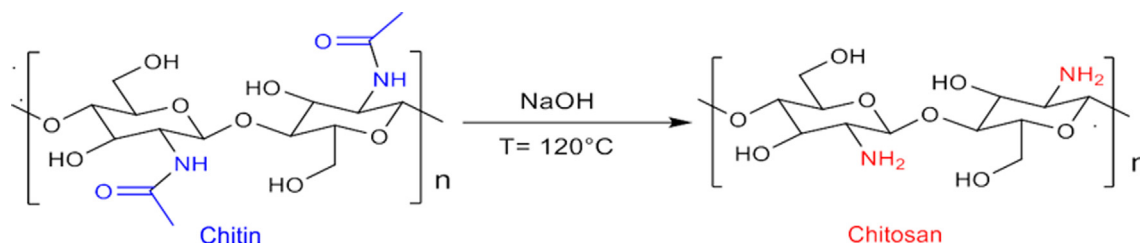
## 2. Materials and methods

### 2.1. Materials

Chitosan, with a deacetylation degree of 83% was successfully prepared in our laboratory through the N-deacetylation process using chitin extracted from shrimp shell waste. Magnesium nitrate,  $Mg(NO_3)_2 \cdot 6H_2O$ , aluminum nitrate,  $Al(NO_3)_3 \cdot 9H_2O$ , sodium hydroxide NaOH, nitric acid  $HNO_3$ , were purchased from LOBA Chemie and benzaldehyde  $C_7H_6O$ , 1-heptanal  $C_7H_{14}O$  and decane



Scheme 1. Aldol condensation reaction of benzaldehyde with 1-heptanal.



**Scheme 2.** Chitosan biopolymer extracted from shrimp shell waste.

$C_{10}H_{22}$  were obtained from Sigma-Aldrich. All of these chemicals are analytical grade (>99.9% purity) and were used as received without further purification. Distilled water was used in the preparation of reactant solutions.

## 2.2. Catalysts preparations

### 2.2.1. Extraction of chitosan (CS)

The extraction of chitosan starts with the collection and cleaning of shrimp shells. The shells undergo a deproteinization process to remove proteins. Then, the chitin in the shells is subjected to deacetylation using a concentrated NaOH solution (12 N) at a temperature of 120 °C for 6 h. This process converts chitin into chitosan. After deacetylation, the resulting alkaline solution is filtered and washed with distilled water until it reaches a neutral pH. Finally, the solution is dried to obtain purified chitosan in the form of a powder. This extraction method is described in detail in a previous works (Ahlafi et al., 2013; Mounir et al., 2021).

### 2.2.2. Synthesis of $MgAl-NO_3$

The bimetallic  $MgAl-NO_3$  LDH with a Mg/Al molar ratio of 3/1, was synthesized using the co-precipitation method. Initially, 0.120 mol of  $Mg(NO_3)_2 \cdot 6H_2O$  and 0.040 mol of  $Al(NO_3)_3 \cdot 9H_2O$  were dissolved in 150 mL of distilled water. This solution was then added to a flask containing 100 mL of distilled water under vigorous stirring at room temperature. A continuous flow of nitrogen gas was maintained during the process. To control the pH of the solution, an aqueous solution of 1.5 M NaOH was progressively added until the pH reached 10. The resulting precipitate was separated from the solution through centrifugation and washed multiple times with distilled water. The obtained catalyst, named  $MgAl-NO_3$ , was left to dry overnight at a temperature of 70 °C.

### 2.2.3. Synthesis of $CS/MgAl-NO_3$ composite

The 10%wt.  $CS/MgAl-NO_3$  catalyst was prepared according to the co-precipitation method. The procedure involved the following steps: A mixture of a concentration of the aqueous solution of  $Mg(NO_3)_2 \cdot 6H_2O$  and  $Al(NO_3)_3 \cdot 9H_2O$  were added to an appropriate weight of chitosan dissolved in 0.1 M nitric acid solution, initially placed in a flask. The pH was then adjusted to pH = 10 by addition of 1.5 M NaOH and the temperature was increased to 70 °C. The mixture was rapidly cooled to room temperature and the flask was left for 24 h without stirring. Afterwards, the precipitate was filtered and washed repeatedly with distilled water until the pH reached 7. Finally, the obtained 10%wt.  $CS/MgAl-NO_3$  catalyst was dried at temperature of 70 °C and stored for further use.

## 2.3. Characterization of catalysts

The crystalline phases of the freshly prepared catalysts were characterized by XRD. The diffractograms were recorded in the  $2\theta$  range from 5 to 70° on a P-XRD Bruker D8-ADVANCE A25 powder diffractometer equipped with a copper anticathode tube and a Cu-K $\alpha$  filter ( $\lambda = 1.5418 \text{ \AA}$ ). The operating voltage and current were

40 kV and 20 mA, respectively. FTIR spectra of the catalysts were recorded in the range of 4000 to 400  $cm^{-1}$  using a SHIMADZU type spectrophotometer (IRAFFINIY-1S), equipped with a Tri-Glycine sulfate detector. The samples were prepared as pellets with 4% of catalysts diluted in KBr. The catalyst thermal stabilities were determined by TGA/DTA using a TA60-SHIMADZU thermal analyzer. The measurements were carried out in air atmosphere in the 25–600 °C temperature range, at a heating rate of 10 °C/min. The catalysts morphologies were analyzed using a scanning electron microscope (SEM) equipped with energy-dispersive X-ray (EDX) analysis. Specifically, images of the catalyst were captured using a JSM-IT500 HR scanning electron microscope at a magnification of approximately 4000 times. An accelerating voltage of approximately 10 kV was applied during the imaging process. Additionally, EDX analysis was performed to gather information about the elemental composition of the catalysts.

The Brunauer-Emmett-Teller (BET) surface area and  $N_2$  adsorption/desorption hystereses were determined at  $-196 \text{ }^\circ\text{C}$  using a Micromeritics ASAP-2010. The Barrett-Joyner-Halenda (BJH) method was used to calculate the pore size distribution. Before the analysis, each catalyst was degassed overnight in vacuum at 100 °C. The acid-base titration method was performed to quantitatively determine the total basicity of the catalysts. This consist of stirring of 100 mg of the catalyst in 10 mL of 0.1 M NaOH solution during 45 min. The resulting suspension was then titrated with a 0.1 M acetic acid solution until the pink color (indicated by phenolphthalein) disappeared, which correspond to the titration of total basicity of the catalyst. The reaction kinetics were monitored using a Shimadzu-2010 gas chromatography instrument (GC), equipped with a 5% diphenyl and 95% dimethyl siloxane capillary DB5 column (30 m length, 0.32 mm inner diameter, and 0.22  $\mu\text{m}$  film thickness) and a flame ionization detector (FID). The GC oven temperature was programmed to increase from 80 to 250 °C at a rate of 10 °C/min, while the injection port and FID were kept at 250 °C during the whole analysis period.

## 2.4. Reaction conditions and analysis

The aldolic condensation reaction between 1-heptanal and benzaldehyde was conducted under 100 W of microwave irradiation which corresponds to a temperature of 90 °C, with reaction times of 10, 20, 30, 40 and 50 min. In each experiment, 10.28 mL of a given ratio of benzaldehyde and 1-heptanal (B/H) $_0$  solution was placed in a 50 mL flask that had a reflux device. The freshly prepared catalyst ( $m = 100 \text{ mg}$ ) was then added to this solution. After a given reaction time  $t$ ,  $x$  mL of the mixture was drawn out by a syringe and the solid was separated from the solution by centrifugation. Then the  $\times$  ml of the reaction solution was diluted in decane/methanol mixture solution (0.1 M), used as an internal standard because decane molecule is known as inactive with respect to the reaction components. Then after, a fraction of 0.1  $\mu\text{L}$  of this diluted solution was injected into the GC column. The reactants/products in the reaction mixture were quantified and the consumption of 1-heptanal, as a function of reaction time,

was used for the calculation of the conversion of 1-heptanal (%) and the selectivity ratio (J/P) following the relations:

$$\text{Conversion of 1-heptanal (\%)} = \frac{[1\text{-heptanal}]_0 - [1\text{-heptanal}]_t}{[1\text{-heptanal}]_0} \times 100 \quad (1)$$

$$\text{Ratio of selectivity (J/P)} = \frac{\text{Selectivity of jasminaldehyde (\%)}}{\text{Selectivity of 2-pentylnon-2-enal (\%)}} \quad (2)$$

To identify the chromatographic peaks of the reactants and of the secondary product of 2-pentylnon-2-enal, obtained by self-condensation of 1-heptanal (carried out under the same conditions as those employed in the reaction studied), they were analyzed individually under the same conditions.

### 3. Results and discussion

#### 3.1. XRD analysis

The X-ray diffraction (XRD) patterns of CS, MgAl-NO<sub>3</sub>, and CS/MgAl-NO<sub>3</sub> are illustrated in Fig. 1. The diffractogram of CS shows reflections at 2θ = 10° and 20°, corresponding to the (020) and (110) diffraction planes of semi-crystalline CS, respectively (Y. Zhang et al., 2005). The XRD pattern of MgAl-NO<sub>3</sub> contains sharp and distinct peaks at around 2θ ≈ 11°, 23° and 36°, which are typical of LDH-like materials. The first peak correspond to the inter-layer space in the LDH, indicating a well-formed of LDH phase (Houssaini et al., 2021). However, the XRD pattern of CS/MgAl-NO<sub>3</sub> showed both the characteristic peaks of MgAl-NO<sub>3</sub> and chitosan, thus confirming the formation of CS/MgAl-NO<sub>3</sub> composite catalyst. It can be observed that the initial peak positions did not change while their intensities have decreased, demonstrating that the CS polymer does not occupy the interlayer space of MgAl-NO<sub>3</sub>, because the value of the parameter c = 3.d<sub>(003)</sub>, corresponding to a basal spacing remains practically unchanged (Table 1). Indeed, this reflects those weak interactions between CS and MgAl-NO<sub>3</sub> occur at its surface, probably through hydrogen bonds or electrostatic type interactions. These interactions affected the shape and the intensity of the peaks, particularly that corresponding to (006) plane, which indicated that the structural order of the initial LDH changed in the composite sample. Moreover, the crystallite sizes (L) was calculated from the Debye-Scherrer formula (Holzwarth & Gibson, 2011):

$$L = \frac{K\lambda}{\beta \cdot \cos(\theta)} \quad (3)$$

Where K is equal to 0.89, β represents the half-width of the X-ray pattern corresponding to the (003) plane at the diffraction angle θ, and λ denotes the wavelength of the X-ray source in angstroms (Å). According to the data presented in Table 1, the calculated crystallite sizes of CS/MgAl-NO<sub>3</sub> were observed to be larger compared to those of MgAl-NO<sub>3</sub>. This variation in crystallite size between the CS/MgAl-NO<sub>3</sub> composite and pure MgAl-NO<sub>3</sub>, demonstrated by the Debye-Scherrer method, can be attributed to the introduction of the CS biopolymer into the composite structure. The presence of the CS biopolymer leads to changes in the crystal growth of MgAl-NO<sub>3</sub> and influences the crystallization processes, ultimately leading to larger crystallite sizes in the composite material.

#### 3.2. FT-IR analysis

Fig. 2 illustrates the FT-IR spectra of CS, MgAl-NO<sub>3</sub> and CS/MgAl-NO<sub>3</sub> composite. The intense absorption band observed in the range of 3400–3500 cm<sup>-1</sup> was attributed to the OH vibration bonds in the samples, while that at 3272 cm<sup>-1</sup> in the spectrum of CS is due to N-H vibrations. This band appears in the spectrum of CS/MgAl-NO<sub>3</sub> at 3268 cm<sup>-1</sup> while it is not observed in MgAl-NO<sub>3</sub> spectrum, indicating that hydrogen bonding interactions were involved between the N-H groups of chitosan and the O-H groups of the LDH. Moreover, infrared spectrum of CS/MgAl-NO<sub>3</sub> reveal additional bands ranged between 1500 and 1700 cm<sup>-1</sup> and 1000–1200 cm<sup>-1</sup>, which are not observed in MgAl-NO<sub>3</sub> spectrum. These regions are characteristic of amide I, amide II and C–O–C, C–O stretching vibration in chitosan (Klein et al., 2016; Moussout et al., 2018), respectively, confirming that the chitosan biopolymer is adsorbed on the surface of MgAl-NO<sub>3</sub> catalyst. This is evidenced by the appearance of the bands at 2876 and 2923 cm<sup>-1</sup>, which correspond to the stretching vibration of C–H bonds in chitosan. In addition, the intense band located at 1382 cm<sup>-1</sup>, due to interlayer nitrate anions in LDH, which overlap with the weak band of amide III in CS, showed no change, suggesting that NO<sub>3</sub> anions remain in internal space of the LDH structure, unaffected by the interactions involved between CS and LDH. In summary, the identification by FT-IR of the different bands of the analyzed samples confirmed the formation of CS/MgAl-NO<sub>3</sub> composite.

#### 3.3. TGA and DTA analysis

TGA and DTA analysis were simultaneously recorded to investigate the thermal stability of CS, MgAl-NO<sub>3</sub> and CS/MgAl-NO<sub>3</sub>. As can be seen in Fig. 3, several phases of weight loss were observed for the prepared samples, which could be attributed to their thermal decomposition. The first weight loss at low temperature (25 °C < T < 150 °C), observed in all the sample thermograms, was due to the desorption of physisorbed water. The desorption temperature and the percentage of weight loss depend on the degree of hydration of each sample. These weight losses lead to the endothermic peaks observed in the DTA curves of CS, MgAl-NO<sub>3</sub> and CS/MgAl-NO<sub>3</sub> at 76, 160 and 101 °C, respectively. Under air flow an oxidative thermal degradation occurs in chitosan which was observed in three stages (weight loss of 52.5%, 17.5% and 15% respectively), in the temperature range of 300–600 °C, indicating the deacetylation of chitosan, vaporization and elimination of volatile products, which generate three exothermic peaks in DTA curve of CS. It is known that the degradation of chitosan starts with amino groups forming unsaturated structures (Moussout et al., 2018). However, during the thermal treatment of MgAl-NO<sub>3</sub>, two weight loss steps (30.5%) were recorded in the temperature range of 200–

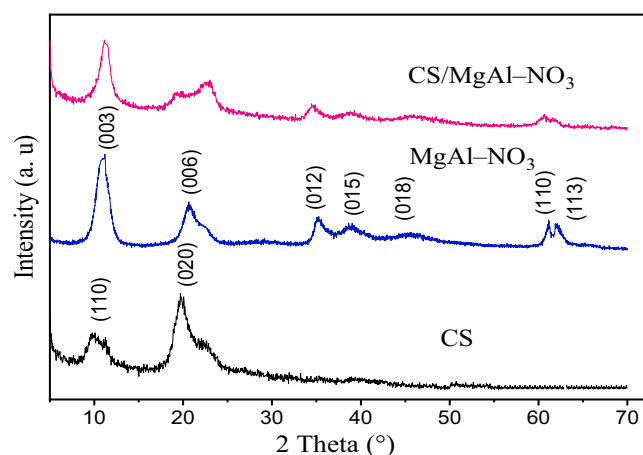
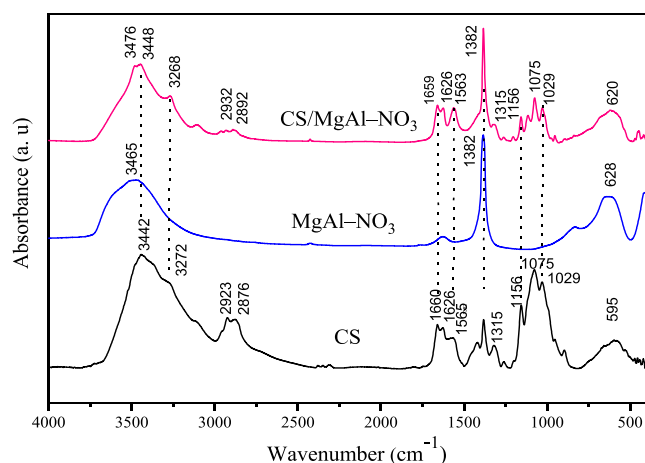


Fig. 1. X-ray diffraction patterns of CS, MgAl-NO<sub>3</sub> and CS/MgAl-NO<sub>3</sub> catalysts.

**Table 1**  
X-ray diffraction analyses of the prepared catalysts.

Catalyst	$\theta_{(003)}$ ( $^{\circ}$ )	$d_{(003)}$ ( $\text{\AA}$ )	$c$ ( $\text{\AA}$ )	$\beta_{(003)}$	$L_{(003)}$ (nm)
MgAl-NO <sub>3</sub>	5.60	7.89	23.67	1.59	5.00
CS/MgAl-NO <sub>3</sub>	5.56	7.95	23.85	1.26	6.24



**Fig. 2.** FT-IR spectra of CS, MgAl-NO<sub>3</sub> and CS/MgAl-NO<sub>3</sub> catalysts.

600 °C leading to a broad endothermic peak centered at  $T = 452$  °C in its DTA curve, which correspond to LDH phase transformations (Prentice et al., 2020): the decomposition of interlayer nitrate anions and the dehydroxylation of LDH structure, which occur successively in this temperature interval. These results are consistent with those of the literature data concerning the thermal decomposition of hydrotalcite materials (Arhzaf et al., 2021; Gholami et al., 2020).

For CS/MgAl-NO<sub>3</sub> composite, the addition of CS into the MgAl-NO<sub>3</sub> resulted in a great difference in the thermal behavior of the composite as compared to MgAl-NO<sub>3</sub> (Fig. 3). The mass loss, at approximately  $T = 160$  °C, is attributed to the removal of loosely bound water molecules from the LDH interlayer, followed by the degradation process of CS in air atmosphere, as described previously for CS alone. The last mass loss at  $T > 500$  °C is due to the oxidation of CS and the dehydroxylation of LDH. The corresponding DTA curve revealed three exothermic peaks during the whole tem-

perature interval, unlike that of MgAl-NO<sub>3</sub>, which indicated that the degradation process of CS/MgAl-NO<sub>3</sub> is gradual and could be linked to the improved thermal stability of CS in the composite, due to the interactions developed between CS and MgAl-NO<sub>3</sub>.

### 3.4. SEM and EDX analysis

The surface properties of CS, MgAl-NO<sub>3</sub>, and CS/MgAl-NO<sub>3</sub> catalysts were characterized using scanning electron microscopy, the results reported in Fig. 4. The SEM analysis of pure CS revealed a smooth and non-porous surface. This suggests that the CS utilized in this study had a homogeneous and pore-free surface. The MgAl-NO<sub>3</sub> based-LDH, exhibited a textured surface comprising small particles that were well-dispersed. These particles had a platelet-like shape and formed aggregates that were uniformly distributed on the surface. In the case of the CS/MgAl-NO<sub>3</sub> composite, the presence of CS on the surface and inside the pores of MgAl-NO<sub>3</sub> led to modifications in the surface properties. Consequently, the porosity of the composite was reduced compared to pure MgAl-NO<sub>3</sub>. This reduction in porosity was confirmed by BET analysis. The observed surface modifications indicate a successful interaction between the two materials in the composite catalyst, suggesting that the CS and MgAl-NO<sub>3</sub> components are effectively integrated.

The findings obtained from SEM analysis were confirmed by EDX analyses. The results of the EDX analyses are presented in Table 2. Specifically, for the CS/MgAl-NO<sub>3</sub> catalyst the characteristic elements identified are carbon at 5.51%, nitrogen at 3.25%, oxygen at 66.26%, magnesium at 19.1% and aluminum at 5.87%. These elements indicate that the composite contains all the elements present in the CS, as well as in the MgAl-NO<sub>3</sub> catalyst. Consequently, the composition of the CS/MgAl-NO<sub>3</sub> composite is a combination of elements derived from two materials.

### 3.5. Surface area, porosity and total basicity

The nitrogen adsorption/desorption behavior of the synthesized MgAl-NO<sub>3</sub> and CS/MgAl-NO<sub>3</sub> are shown in Fig. 5. In both cases, the

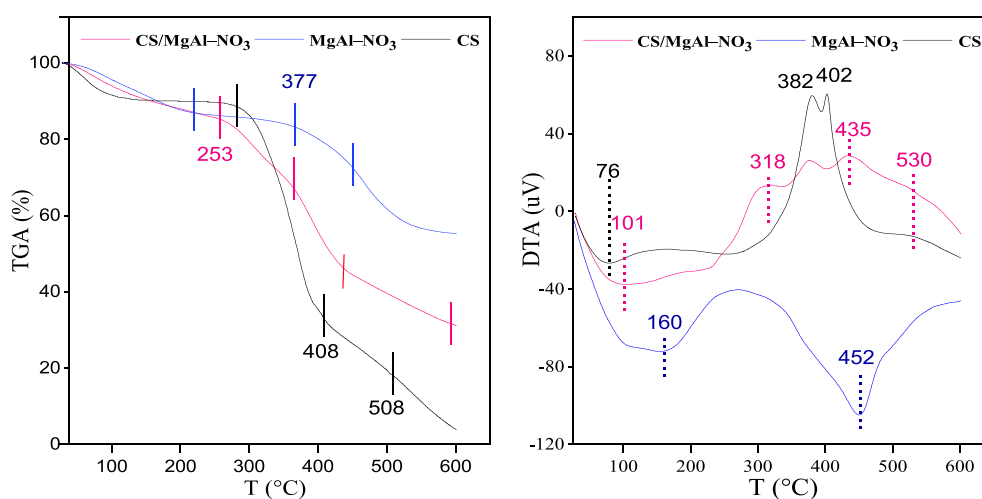


**Fig. 3.** TGA-DTA curves of CS, MgAl-NO<sub>3</sub> and CS/MgAl-NO<sub>3</sub> catalysts.

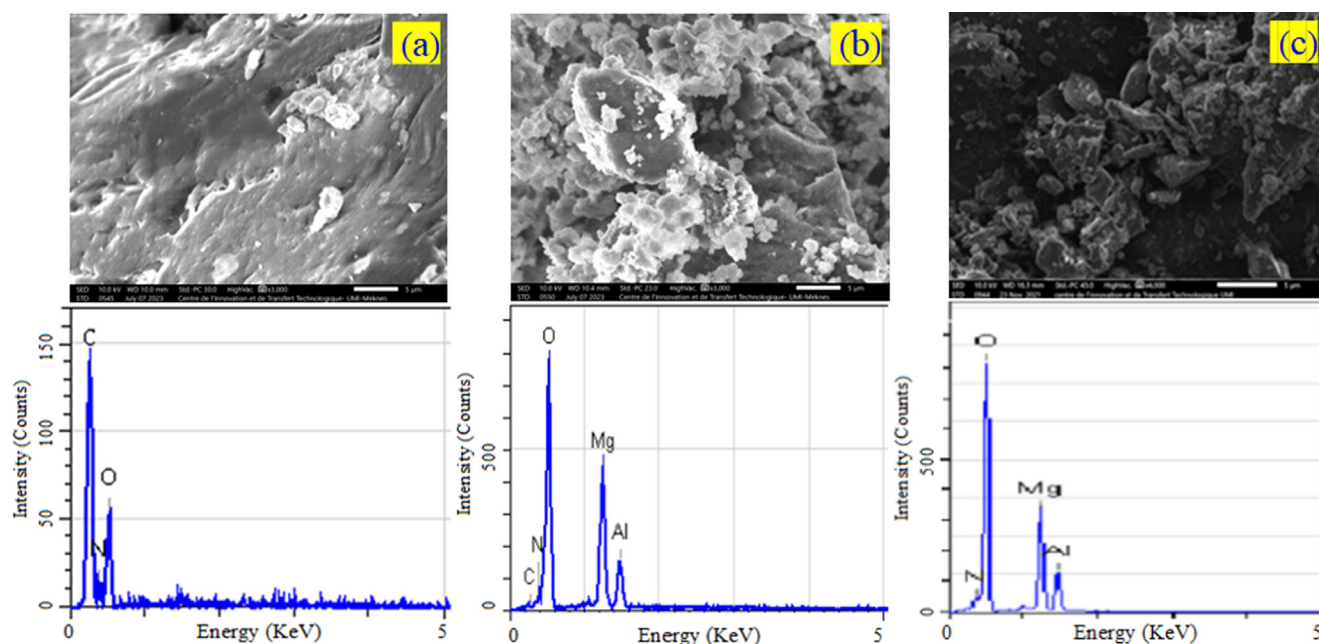


Fig. 4. SEM images at 5  $\mu\text{m}$ , and EDX analysis of (a) CS, (b) CS/MgAl-NO<sub>3</sub> and (c) MgAl-NO<sub>3</sub> catalysts.

Table 2  
EDX elemental data analysis of the catalysts.

Catalyst	Atomic percent in (%)				
	C	N	O	Mg	Al
CS	39.17	12.16	48.67	–	–
MgAl-NO <sub>3</sub>	–	1.98	69.42	21.44	7.16
CS/MgAl-NO <sub>3</sub>	5.51	3.25	66.26	19.11	5.87

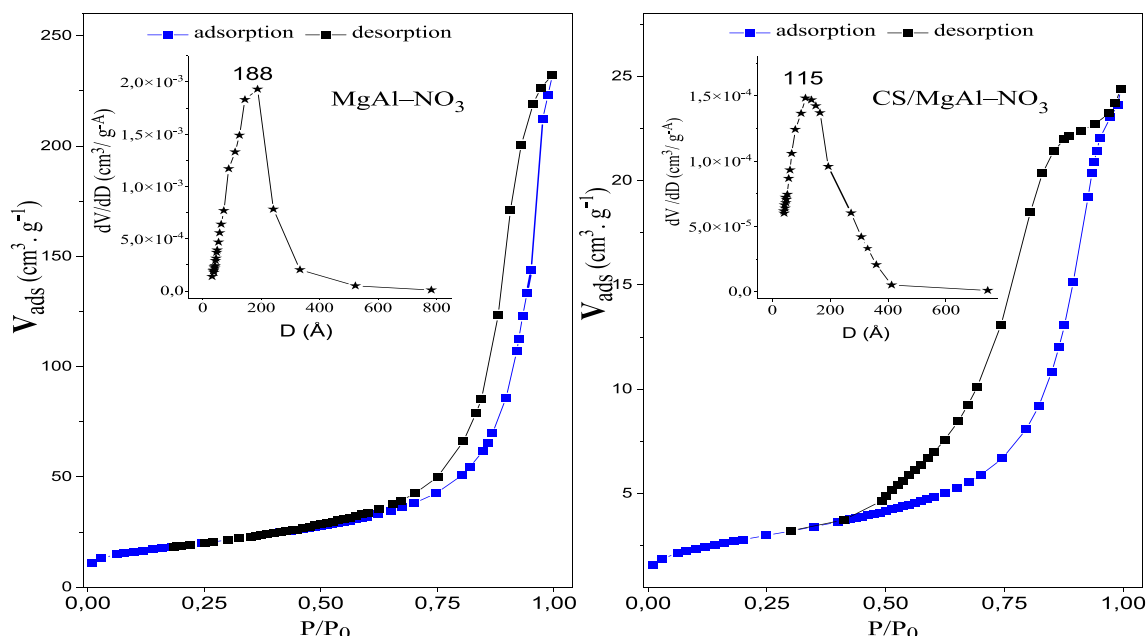


Fig. 5. N<sub>2</sub> adsorption–desorption isotherms and pore diameter distributions for the MgAl-NO<sub>3</sub> and CS/MgAl-NO<sub>3</sub> catalysts.

shape of the isotherms is of type IV for the two samples, according to the international union of pure and applied chemistry classification (IUPAC), with the presence of hysteresis, indicating their

mesoporous nature (Arhzaf et al., 2021). However the nitrogen adsorption follows an isotherm of type IIIb, according to the classification proposed by Rouquerol et al. (Rouquerol et al., 1989) and a

**Table 3**  
Textural parameters and basicity of the synthesized catalysts.

Catalyst	Specific surface area ( $\text{m}^2 \cdot \text{g}^{-1}$ )	Pore volume ( $\text{cm}^3 \cdot \text{g}^{-1}$ )	Average pore diameter ( $\text{\AA}$ )	Basicity ( $\text{mmol} \cdot \text{g}^{-1}$ )
MgAl-NO <sub>3</sub>	95	0.353	188	1.32
CS/MgAl-NO <sub>3</sub>	20	0.038	115	1.36

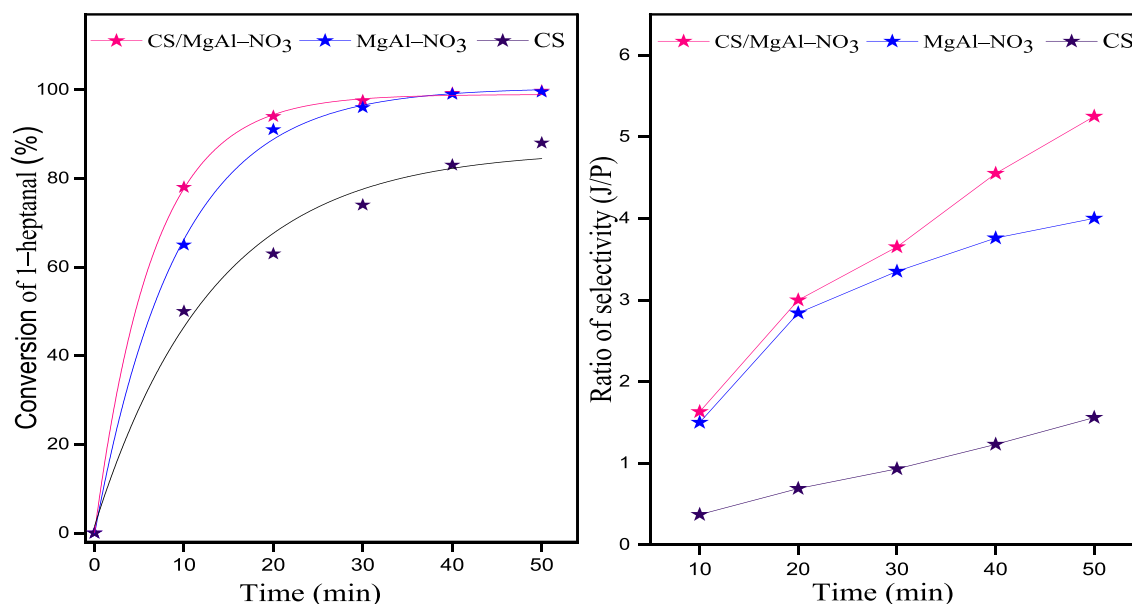


**Fig. 6.** Conversion of 1-heptanal over the three catalysts and ratio of selectivity (J/P) as a function of reaction time: molar ratio of (B/H)<sub>0</sub> = 5:1, m = 100 mg of the catalyst, Power 100 W and T = 90 °C.

H3-type hysteresis loop for the desorption. Comparatively to the type IV, the isotherms of type IIb do not present a plateau at high P/P<sub>0</sub> values, and the LDH materials adopt generally these characteristics (C. Y. Zhang et al., 2019). The curve shape comes from nitrogen physisorption taking place between the aggregates of particles, and the closing of the desorption part is accompanied by a pronounced decrease in the adsorbed volume (at a relative pressure P/P<sub>0</sub> = 0.45). This corresponds to the filling of small mesopores (Rouquerol et al., 1989). The textural parameters of the catalysts, are presented in Table 2. It can be shown that the specific surface area of MgAl-NO<sub>3</sub> (95 m<sup>2</sup>·g<sup>-1</sup>) is higher than that of CS/MgAl-NO<sub>3</sub> (20 m<sup>2</sup>·g<sup>-1</sup>), and the pore volume was decreased from 0.353 cm<sup>3</sup>·g<sup>-1</sup> to 0.038 cm<sup>3</sup>·g<sup>-1</sup>, due to the penetration of CS polymer inside the pores of MgAl-NO<sub>3</sub>, which causes a notable decrease in its pore diameter from 188 to 115 Å.

The total basicity of the synthesized catalysts was measured quantitatively using the acid-base titration method (Sahu et al., 2013), and the Hammett indicator method (Cantrell et al., 2005; Devi et al., 2018). The basicity is expressed in units of mmole·g<sup>-1</sup> calculated from the titer of acidic acid solution required for the amount of each solid sample, as follows:

$$\text{Basicity} = C_{AA} \times \frac{\Delta V_{AA}}{m_{\text{Cat}}} \quad (4)$$

Where C<sub>AA</sub> represents the concentration of the standard acetic acid solution, ΔV<sub>AA</sub> is the difference in volume between the acetic acid solution consumed by the solution containing the catalyst and the blank at equivalence, and m<sub>Cat</sub> represents the mass of the catalyst used in the test. From Table 3, MgAl-NO<sub>3</sub> and CS/MgAl-NO<sub>3</sub> showed the basicity of 1.32 and 1.36 mmol·g<sup>-1</sup> respectively, which

seems to be identical. However, the basicity calculated with respect to the specific surface area becomes (1.32/95 = 0.014 mmol·m<sup>-2</sup>) for MgAl-NO<sub>3</sub> and (1.36/20 = 0.068 mmol·m<sup>-2</sup>) for CS/MgAl-NO<sub>3</sub>, which shows the composite has a good basicity due to (-OH) and (-NH<sub>2</sub>) groups of CS biopolymer, located on the surface. The increase in the basicity of this catalyst could be beneficial for aldol condensation of benzaldehyde with 1-heptanal.

## 4. Kinetic studies

### 4.1. Evaluation of the catalytic activity of the catalysts

Aldol condensation reaction between benzaldehyde and 1-heptanal was chosen as a model reaction to evaluate the catalytic activity of CS, MgAl-NO<sub>3</sub> and CS/MgAl-NO<sub>3</sub> basic catalysts, under microwave irradiation and solvent free conditions. The effect of reaction parameters, such as the amount of catalyst, benzaldehyde to 1-heptanal molar ratio, and reaction temperature on the conversion of 1-heptanal and the selectivity of jasminaldehyde was evaluated. Apparently, Fig. 6 summarized the results of the conversion of 1-heptanal (%) and the ratio of selectivity (J/P) obtained versus the time of reaction over the three catalysts. The conversion of 1-heptanal increased with the reaction time and reaches 97.5%, 96% and 74% after t = 30 min for CS/MgAl-NO<sub>3</sub>, MgAl-NO<sub>3</sub> and CS catalysts, respectively. On the other side the selectivity of jasminaldehyde also increased when the reaction time increased. Noticeably, the CS/MgAl-NO<sub>3</sub> catalyst presents the better conversion and ratio of selectivity, compared to those of MgAl-NO<sub>3</sub> and CS catalysts. This result indicated that the catalysts promote the

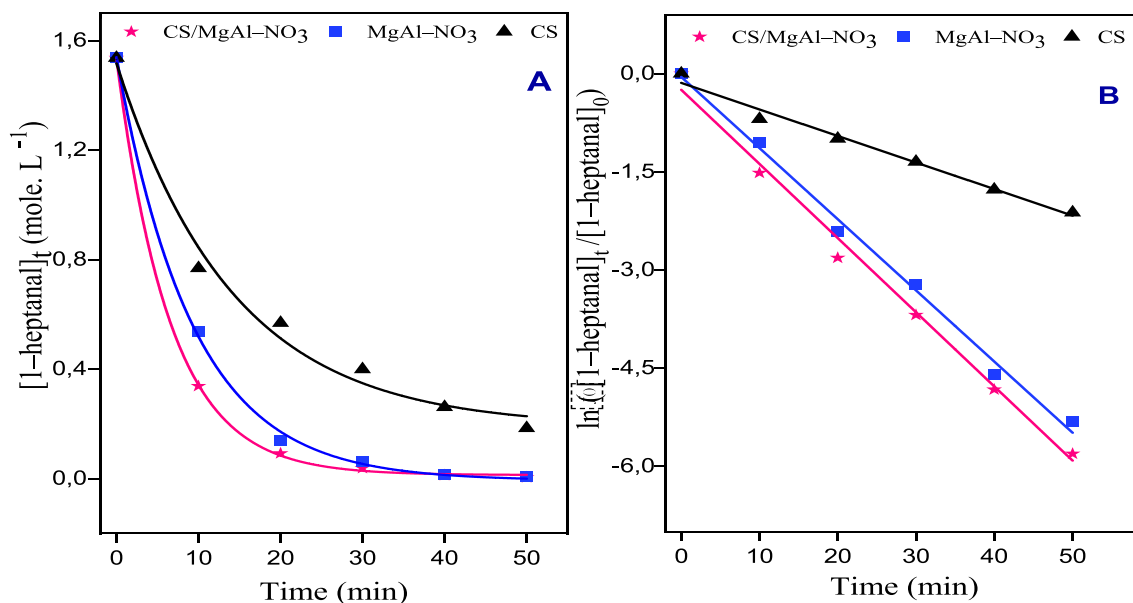


Fig. 7. Kinetic of 1-heptanal consumption vs the time of reaction over: CS/MgAl-NO<sub>3</sub>, MgAl-NO<sub>3</sub> and CS catalysts.

Table 4

Conversion of 1-heptanal, selectivity ratio (J/P), and initial reaction rate of the reaction.

Catalyst	Conversion of 1-heptanal (%)	Selectivity ratio (J/P)	Initial rate (mol. L <sup>-1</sup> . min <sup>-1</sup> )	K <sub>app</sub> (min <sup>-1</sup> )
CS	88	1.56	0.087	0.040
MgAl-NO <sub>3</sub>	99.5	4.00	0.160	0.108
CS/MgAl-NO <sub>3</sub>	99.7	5.25	0.208	0.113

**Reaction conditions:** 79 mmole of benzaldehyde, 15.8 mmole of 1-heptanal, m = 100 mg of the catalyst, Power 100 W, T = 90 °C and reaction time: 50 min.

condensation of heptanal with benzaldehyde than the self-condensation of 1-heptanal.

Additionally, an analysis was conducted to determine the kinetic parameters of the reaction, including the reaction order and rate constant. To achieve this, the initial rate ( $r_0$ ) of 1-heptanal disappearance was measured at various time intervals, expressed in terms of mol. L<sup>-1</sup> of reactants per unit time. As depicted in Fig. 7A, the obtained curves demonstrate that the decrease in 1-heptanal follows an exponential decay pattern, indicating a first-order kinetics behavior. Consequently, the initial reaction rate as a function of time can be expressed as follows:

$$r_0 = \frac{-d[1\text{-heptanal}]}{dt} = k.[1\text{-heptanal}]^\alpha.[\text{benzaldehyde}]^\beta = k_{app}. [1\text{-heptanal}] \quad (5)$$

Where  $\alpha$  and  $\beta$  represent the partial orders corresponding to each reactant and  $K_{app} = k.[\text{benzaldehyde}]^\beta$  is the apparent rate constant because benzaldehyde is present in excess in the reaction medium. The integrated form of equation (5) is:  $[1\text{-heptanal}]_t = [1\text{-heptanal}]_0 \cdot \exp(-K_{app} \cdot t)$ .

The plot of  $\ln\left(\frac{[1\text{-heptanal}]_t}{[1\text{-heptanal}]_0}\right) = -K_{app} \cdot t$ , lead to the straight lines as shown in Fig. 7B, which confirm that the aldol condensation reaction follows a pseudo-first-order law. The apparent rate constants values, determined from the slopes of the previous lines, are given in Table 4. It can be shown that the CS/MgAl-NO<sub>3</sub> catalyst achieved a higher value, which is about 1.3 and 2.4 times of those of MgAl-NO<sub>3</sub> and CS, respectively, due to the high density of the active basic

sites on its surface. Thus, further optimization experiments were performed by the catalyst CS/MgAl-NO<sub>3</sub>.

#### 4.2. Effect of reaction temperature

In order to better understand the aldol condensation of benzaldehyde and 1-heptanal over CS/MgAl-NO<sub>3</sub> catalyst, it was visually observed that the conversion (%) and ratio of selectivity (J/P) increases with an increase in reaction temperature (Fig. 8), clearly indicating that higher temperatures favor the aldol condensation of benzaldehyde and 1-heptanal. It is evident that the effect of reaction temperature has a significant influence on the kinetics of this reaction. These results are consistent with the obtained findings. For example, at a temperature of 40 °C and a reaction time of 50 min, the conversion of 1-heptanal was only 85%, with a selectivity ratio (J/P) of approximately 1.08. However, when the reaction temperature was increased to 60 °C, the conversion increased to 93%, and the selectivity ratio (J/P) increased to 2.7. Furthermore, when the temperature was further raised from 60 °C to 90 °C, there were significant improvements in both the conversion of 1-heptanal and the selectivity ratio (J/P) compared to the results obtained at 60 °C. Specifically, at a temperature of 90 °C, the conversion of 1-heptanal reached 99.7%, and the selectivity ratio (J/P) was measured to be 5.25. These experimental results indicate that increasing the temperature has a positive effect on the condensation reaction between benzaldehyde and 1-heptanal in the presence of the CS/MgAl-NO<sub>3</sub> catalyst. As a result, the optimal reaction temperature and duration for this specific reaction were

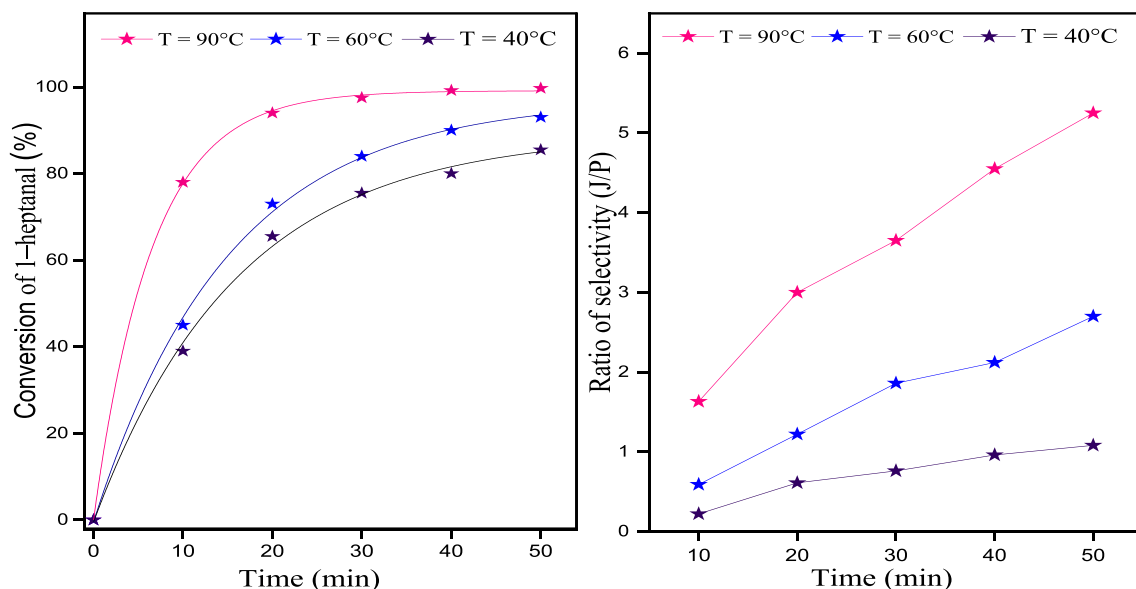


Fig. 8. Effect of reaction temperature on conversion of 1-heptanal and ratio of selectivity (J/P) versus the reaction time over CS/MgAl-NO<sub>3</sub> catalyst.

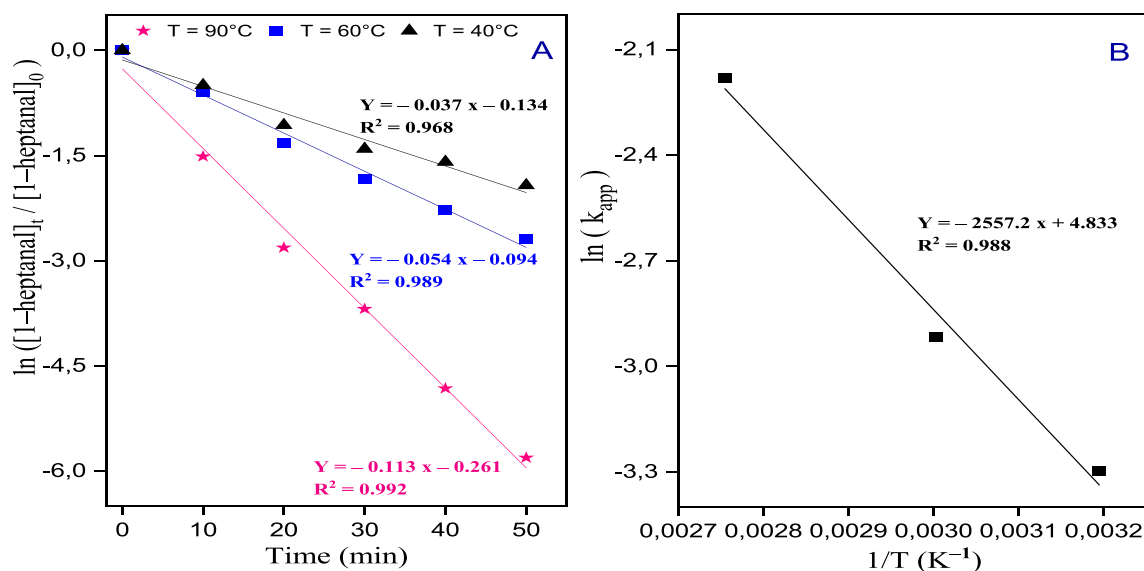


Fig. 9. Kinetic profiles of aldol condensation of benzaldehyde and 1-heptanal over CS/MgAl-NO<sub>3</sub> catalyst.

determined to be 90 °C and 50 min, respectively. These conditions were identified as the most favorable, as they resulted in the highest conversion rate of 1-heptanal and the desired product selectivity.

The calculation of the activation energy ( $E_a$ ) for the aldol condensation reaction between benzaldehyde and 1-heptanal employing the CS/MgAl-NO<sub>3</sub> catalyst, the apparent rate constant ( $k_{app}$ ) was determined at various temperatures (40, 60, and 90 °C). The conversion of 1-heptanal (%) was assumed to follow a pseudo-first-order reaction, as depicted in Fig. 9A. The Arrhenius Eq. (6), was employed in the analysis.

$$\ln k = \ln A - (E_a/RT) \quad (6)$$

In the Eq. (6),  $k$  represents the rate constant,  $A$  is the Arrhenius constant,  $R$  is the ideal gas constant (8.314 J mol<sup>-1</sup> K<sup>-1</sup>), and  $T$  is the temperature in Kelvin. By plotting  $\ln(k_{app})$  against  $1/T$ , the apparent activation energy can be determined from the slope of

the resulting line. Furthermore, the activation energy for the reaction catalyzed by the CS/MgAl-NO<sub>3</sub> catalyst was obtained from the slope of the Arrhenius plot, as shown in Fig. 9B. The calculated activation energy was found to be 21.25 kJ/mol. The relatively low value of the activation energy further confirms the high effectiveness of the catalyst in promoting the aldol condensation of benzaldehyde and 1-heptanal. This suggests that the catalyst significantly lowers the energy barrier for the reaction, facilitating the formation of the desired product.

#### 4.3. Effect of benzaldehyde/1-heptanal molar ratio

To examine the influence of molar ratio of benzaldehyde to 1-heptanal on the conversion of 1-heptanal and the selectivity of jasminaldehyde, the study was performed over CS/MgAl-NO<sub>3</sub> catalyst using three molar ratios of 5:5, 5:2 and 5:1, while other parameters were kept constants. As seen in Fig. 10, the best conversion of 1-

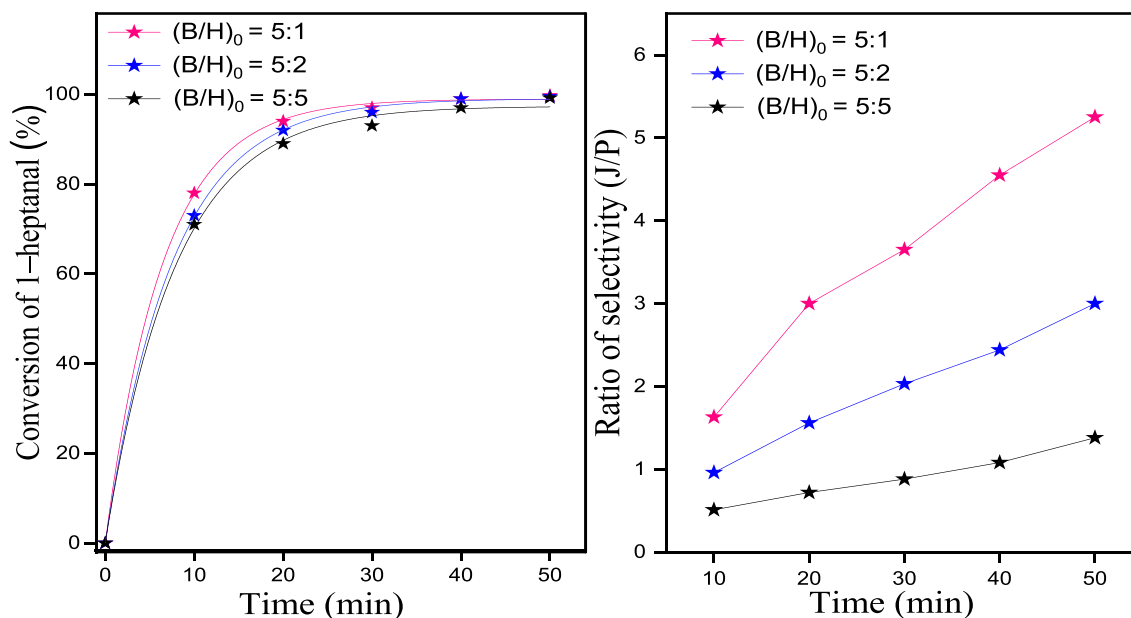


Fig. 10. Effect of molar ratio  $(B/H)_0$  on the conversion of 1-heptanal and ratio of selectivity  $(J/P)$  using CS/MgAl-NO<sub>3</sub> catalyst for the synthesis of jasminaldehyde.

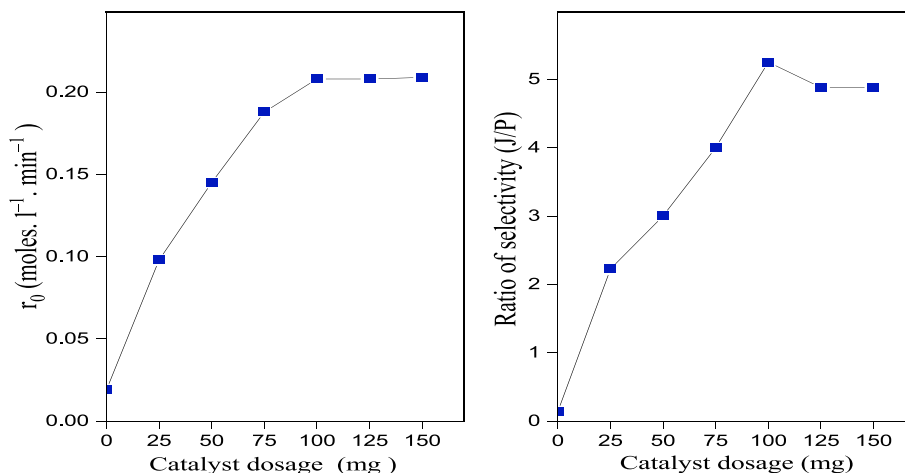


Fig. 11. Effect of catalyst dosage on the initial rate of reaction and selectivity ratio  $(J/P)$  over CS/MgAl-NO<sub>3</sub> catalyst.

heptanal with a higher selectivity ratio  $(J/P)$  are obtained with a molar ratio of  $(B/H)_0 = 5:1$ . This indicates that the molar ratio of  $(B/H)_0$  has a significant impact on both the conversion of 1-heptanal and the selectivity to jasminaldehyde. For example, the ratio of selectivity  $(J/P)$  increases from 1.38 to 5.25 with the increase of  $(B/H)_0$  ratio from 5:5 to 5:1 respectively, after 50 min of reaction time, consequently, the higher concentration of benzaldehyde in the reaction mixture, decreased the possibility of self-condensation of heptanal, in favor of the aldol condensation of benzaldehyde with 1-heptanal to jasminaldehyde. The decrease in molar ratio up to 5:5 hinders the active sites on the catalyst thus reducing the conversion, which could be due to the competitive adsorption of benzaldehyde and 1-heptanal on the adsorption sites at CS/MgAl-NO<sub>3</sub> surface, because the benzaldehyde is present in excess in the reaction medium, which favors its adsorption over that of heptanal. As the concentration of benzaldehyde increased, the number of available sites for adsorption of heptanal decreased. The same behavior was reported by other authors (Adwani et al.,

2015; Hamza & Nagaraju, 2015; Sudheesh et al., 2011). Hence, the molar ratio of  $(B/H)_0 = 5:1$  was selected as the optimal ratio for the aldol condensation of benzaldehyde and 1-heptanal.

#### 4.4. Effect of catalyst dosage

In order to understand the amount of CS/MgAl-NO<sub>3</sub> catalyst effect on the selectivity to jasminaldehyde, the aldol condensation reaction was carried out for benzaldehyde to 1-heptanal ratio of 5:1, and varying the catalyst amount from 25 to 150 mg. The corresponding results are shown in Fig. 11, where it can be observed that the initial reaction rate increased up to 0.208 mol. L<sup>-1</sup>. min<sup>-1</sup> for the catalyst amount of 100 mg and further increase in catalyst dosage to 150 mg leads no significant change in the initial reaction rate. The increase is likely due to the availability of the active basic sites, which reaches an optimal number useful for the aldol condensation reaction. This behavior has also been reported by many authors, indicating that increasing the amount of catalyst at

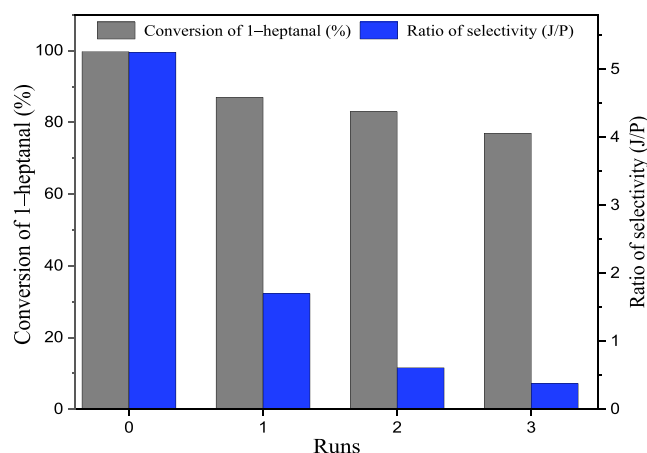


**Fig. 12.** Reusability of the CS/MgAl-NO<sub>3</sub> catalyst in aldol condensation of benzaldehyde and 1-heptanal. (Reaction conditions: 79 mmole of benzaldehyde, 15.8 mmole of 1-heptanal, Power 100 W, T = 90 °C, and reaction time 50 min).

level > 200 mg, leads to a decrease in the selectivity towards jasminaldehyde. This may be due to the increase of the particle sizes, with more amount of the catalyst, exceeding the optimal amount, where the particles remain well dispersed. Consequently, access to the basic sites becomes easy, thus promoting the conversion and the selectivity towards the jasminaldehyde. The decrease of the latter parameters with the amount of the catalyst can also be due to the increase in the number of acid sites.

#### 4.5. Catalyst regeneration tests

The evaluation of solid catalysts for industrial applications often presents a challenge due to the issue of catalyst reusability. In light of this, the reusability of CS/MgAl-NO<sub>3</sub> in the studied reaction was investigated by conducting four successive cycles under the previously determined optimal reaction conditions. After each catalytic reaction, the catalyst is recovered from the reaction solution by centrifugation, washed several times with methanol to remove the reactants/products from its surface, then dried at temperature of 60 °C for 5 h. The results of 1-heptanal conversion and ratio of selectivity (J/P) are presented in Fig. 12. Compared to the fresh catalyst, the conversion decreases from 99.7% to 77% after three successive cycles, while the selectivity ratio (J/P) significantly decreases from 5.25 to 0.38. These results indicated that the initial catalytic activity of the recovered CS/MgAl-NO<sub>3</sub> catalyst was not conserved after each cycle. This loss is mainly due to the diminution in the number of active basic sites involved in aldol condensation of benzaldehyde and 1-heptanal reaction, which can be caused by the loss of a small amount of catalyst during the separation process, as well as to the products/reactants blocked inside the catalyst pores, not fully desorbed during its drying at T = 60 °C.

## 5. Conclusions

The MgAl-NO<sub>3</sub> LDH catalyst and its functionalized form with chitosan (CS/MgAl-NO<sub>3</sub>) were successfully synthesized under a nitrogen (N<sub>2</sub>) atmosphere using the co-precipitation method at a constant basic pH of 10. The catalysts were characterized using XRD, TGA/DTA, SEM/EDX and BET adsorption/desorption methods. The characterization revealed that the impregnation of MgAl-NO<sub>3</sub> with CS resulted in an increase in particle size, leading to a decrease in surface area and alterations in thermal behavior. The catalysts exhibited excellent performance under solvent-free conditions and microwave irradiation with a power of 100 W. The

optimized reaction conditions included using 100 mg of catalyst, a benzaldehyde to 1-heptanal molar ratio of 5:1 and a temperature of 90 °C. Under these conditions, the aldol condensation of benzaldehyde with 1-heptanal resulted in the highest conversion of 1-heptanal and selectivity to jasminaldehyde. The catalytic performance of CS/MgAl-NO<sub>3</sub> was superior to that of MgAl-NO<sub>3</sub>. This can be attributed to the additional amino (-NH<sub>2</sub>) and hydroxyl (-OH) basic sites provided by CS on the catalyst's surface, as confirmed by the titration method. These additional sites contributed to an increased initial reaction rate. The CS/MgAl-NO<sub>3</sub> achieved the highest selectivity for jasminaldehyde (84%) when the molar ratio of benzaldehyde to 1-heptanal was 5:1. The aldol condensation reaction to jasminaldehyde followed pseudo-first-order kinetics with respect to the concentration of 1-heptanal. The excellent catalytic efficiency of CS/MgAl-NO<sub>3</sub> in the aldol condensation reaction between benzaldehyde and 1-heptanal was confirmed by the low activation energy value obtained from kinetic studies, which was measured to be 21.25 kJ/mol. Furthermore, the catalysts used in the reaction could be easily regenerated through a simple process and reused for subsequent reactions, indicating their potential for sustainable and efficient catalytic applications.

## Research funding

This research was sustained by the Ministry of Higher Education and the National Center for Scientific and Technical Research (CNRST), Morocco.

## Declaration of Competing Interest

The authors declare that they have no known competing financial interests or personal relationships that could have appeared to influence the work reported in this paper.

## Acknowledgments

We are grateful to thank the Laboratory of Chemistry and Biology Applied to the Environment, affiliate at the CNRST, Research Team of Materials and Applied Catalysis at Moulay Ismail University in Morocco.

## References

- Abd El-Monaem, E.M., Elshishini, H.M., Bakr, S.S., El-Aqapa, H.G., Hosny, M., Andaluri, G., El-Subruiti, G.M., Omer, A.M., Eltaweil, A.S., 2023. A comprehensive review on LDH-based catalysts to activate persulfates for the degradation of organic pollutants. *Npj Clean Water* 6 (1). <https://doi.org/10.1038/s41545-023-00245-x>.
- Abdelkrim, E.K., 2015. Chitosan as a sustainable organocatalyst: A concise overview. *ChemSusChem* 8 (2), 217–244. <https://doi.org/10.1002/cssc.201402718>.
- Adwani, J.H., Khan, N.U.H., Shukla, R.S., 2015. An elegant synthesis of chitosan grafted hydrocalcite nano-bio composite material and its effective catalysis for solvent-free synthesis of jasminaldehyde. *RSC Adv.* 5 (115), 94562–94570. <https://doi.org/10.1039/c5ra16927e>.
- Ahlafi, H., Moussout, H., Boukhilfi, F., Echetna, M., Bennani, M.N., My Slimane, S., 2013. Kinetics of N-Deacetylation of Chitin Extracted from Shrimp Shells Collected from Coastal Area of Morocco. *Mediterranean Journal of Chemistry* 2 (3), 503–513. [10.13171/mjc.2.3.2013.22.01.20](https://doi.org/10.13171/mjc.2.3.2013.22.01.20).
- Alghamdi, K.S., Ahmed, N.S.I., Bakhotmah, D., Mokhtar, M., 2019. Chitosan Decorated Copper Nanoparticles as Efficient Catalyst for Synthesis of Novel Quinoline Derivatives. *J. Nanosci. Nanotechnol.* 20 (2), 890–899. <https://doi.org/10.1166/jnn.2020.16923>.
- Alzhrani, G., Ahmed, N.S., Aazam, E.S., Saleh, T.S., Mokhtar, M., 2019. Novel Efficient Pd-Free Ni-Layered Double Hydroxide Catalysts for a Suzuki C-C Coupling Reaction. *ChemistrySelect* 4 (27), 7904–7911. <https://doi.org/10.1002/slct.201900890>.
- Arhzaf, S., Bennani, M.N., Abouarnadasse, S., Houssaini, J., Ziyat, H., Qabaqous, O., 2021. Solvent-free aldol condensation of furfural and acetone on calcined Mg-Al hydroxalicates. *Moroccan Journal of Chemistry* 9 (3), 614–627. [10.48317/IMIST.PRSM/morjchem-v9i3.23587](https://doi.org/10.48317/IMIST.PRSM/morjchem-v9i3.23587).

- Bernard, E., Zucha, W.J., Lothenbach, B., Mäder, U., 2022. Stability of hydrotalcite (Mg-Al layered double hydroxide) in presence of different anions. *Cem. Concr. Res.* 152(May, 2021). <https://doi.org/10.1016/j.cemconres.2021.106674>.
- Cantrell, D.G., Gillie, L.J., Lee, A.F., Wilson, K., 2005. Structure-reactivity correlations in MgAl hydrotalcite catalysts for biodiesel synthesis. *Appl. Catal. A* 287 (2), 183–190. <https://doi.org/10.1016/j.apcata.2005.03.027>.
- Chatterjee, A., Bharadiya, P., Hansora, D., 2019. Layered double hydroxide based bionanocomposites. *Appl. Clay Sci.* 177 (April), 19–36. <https://doi.org/10.1016/j.clay.2019.04.022>.
- Chen, Y., Zhou, T., Fang, H., Li, S., Yao, Y., He, Y., 2015. A novel preparation of nano-sized hexagonal Mg(OH)<sub>2</sub>. *Procedia Eng.* 102, 388–394. <https://doi.org/10.1016/j.proeng.2015.01.169>.
- Debecker, D.P., Gaigneaux, E.M., Busca, G., 2009. Exploring, tuning, and exploiting the basicity of hydrotalcites for applications in heterogeneous catalysis. *Chem. A Eur. J.* 15 (16), 3920–3935. <https://doi.org/10.1002/chem.200900060>.
- Devi, R., Begum, P., Bharali, P., Deka, R.C., 2018. Comparative Study of Potassium Salt-Loaded MgAl Hydrotalcites for the Knoevenagel Condensation Reaction [Research-article]. *ACS Omega* 3 (6), 7086–7095. <https://doi.org/10.1021/acsomega.8b00767>.
- Eltaweil, A.S., Bakr, S.S., Abd El-Monaem, E.M., El-Subruiti, G.M., 2023. Magnetic hierarchical flower-like Fe<sub>3</sub>O<sub>4</sub>@ZIF-67/CuNiMn-LDH catalyst with enhanced redox cycle for Fenton-like degradation of Congo red: optimization and mechanism. *Environ. Sci. Pollut. Res.* 30 (30), 75332–75348. <https://doi.org/10.1007/s11356-023-27430-2>.
- Fan, A., 2020. Acid–base bifunctional magnesium oxide catalyst prepared from a simple hydrogen peroxide treatment for highly selective synthesis of jasminaldehyde. *Energy Sources Part A* 42 (20), 2501–2515. <https://doi.org/10.1080/15567036.2019.1607949>.
- Ganga, V.S.R., Abdi, S.H.R., Kureshy, R.I., Khan, N.U.H., Bajaj, H.C., 2016. P-Toluene sulfonic acid (PTSA)-MCM-41 as a green, efficient and reusable heterogeneous catalyst for the synthesis of jasminaldehyde under solvent-free condition. *J. Mol. Catal. A Chem.* 420, 264–271. <https://doi.org/10.1016/j.molcata.2016.04.030>.
- Gholami, Z., Tišler, Z., Vondrová, P., Velvarská, R., Štěpánek, K., 2020. Solvent-free synthesis of jasminaldehyde in a fixed-bed flow reactor over mg-al mixed oxide. *Catalysts* 10 (9), 1–14. <https://doi.org/10.3390/catal10091033>.
- Hajek, J., Vandichel, M., Van De Voorde, B., Bueken, B., De Vos, D., Waroquier, M., Van Speybroeck, V., 2015. Mechanistic studies of aldol condensations in UiO-66 and UiO-66-NH<sub>2</sub> metal organic frameworks. *J. Catal.* 331 (Figure 1), 1–12. <https://doi.org/10.1016/j.jcat.2015.08.015>.
- Hamza, A., Nagaraju, N., 2015. Amorphous metal–aluminophosphate catalysts for aldol condensation of n-heptanal and benzaldehyde to jasminaldehyde. *Cuihua Xuebao/Chinese Journal of Catalysis* 36 (2), 209–215. [https://doi.org/10.1016/S1872-2067\(14\)60206-0](https://doi.org/10.1016/S1872-2067(14)60206-0).
- Holzwarth, U., Gibson, N., 2011. The Scherrer equation versus the “Debye-Scherrer equation”. *Nat. Nanotechnol.* 6 (9), 534. <https://doi.org/10.1038/nnano.2011.145>.
- Houssaini, J., Bennani, M.N., Ziyat, H., Arhzaif, S., Qabaqous, O., Amhoud, A., 2021. Study of the Catalytic Activity of the Compounds Hydrotalcite Mg-Al Treated by Microwave in the Self-Condensation of Acetone. *International Journal of Analytical Chemistry* 2, 1–10. <https://doi.org/10.1155/2021/1551586>.
- Klein, M.P., Hackenhaar, C.R., Lorenzoni, A.S.G., Rodrigues, R.C., Costa, T.M.H., Ninow, J.L., Hertz, P.F., 2016. Chitosan crosslinked with genipin as support matrix for application in food process: Support characterization and β-d-galactosidase immobilization. *Carbohydr. Polym.* 137, 184–190. <https://doi.org/10.1016/j.carbpol.2015.10.069>.
- Mokhtar, M., Alzhrani, G., Aazam, E.S., Saleh, T.S., Al-Faiif, S., Panja, S., Maiti, D., 2021. Synergistic Effect of NiLDH@YZ Hybrid and Mechanochemical Agitation on Glaser Homocoupling Reaction. *Chem. A Eur. J.* 27 (34), 8875–8885. <https://doi.org/10.1002/chem.202100018>.
- Molnár, Á., 2019. The use of chitosan-based metal catalysts in organic transformations. *Coord. Chem. Rev.* 388, 126–171. <https://doi.org/10.1016/j.ccr.2019.02.018>.
- Mounir, C., Ahlafi, H., Aazza, M., Moussout, H., Mounir, S., 2021. Kinetics and Langmuir-Hinshelwood mechanism for the catalytic reduction of para-nitrophenol over Cu catalysts supported on chitin and chitosan biopolymers. *React. Kinet. Mech. Catal.* 134 (1), 285–302. <https://doi.org/10.1007/s11144-021-02066-w>.
- Moussout, H., Ahlafi, H., Aazza, M., Amehrouq, A., 2018. Al<sub>2</sub>O<sub>3</sub>/chitosan nanocomposite: Preparation, characterization and kinetic study of its thermal degradation. *Thermochim Acta* 668 (May), 169–177. <https://doi.org/10.1016/j.tca.2018.08.023>.
- Narasimharao, K., Al-Sabban, E., Saleh, T.S., Gallastegui, A.G., Sanfiz, A.C., Basahel, S., Al-Thabaiti, S., Alyoubi, A., Obaid, A., Mokhtar, M., 2013. Microwave assisted efficient protocol for the classic Ullmann homocoupling reaction using Cu-Mg-Al hydrotalcite catalysts. *J. Mol. Catal. A Chem.* 379, 152–162. <https://doi.org/10.1016/j.molcata.2013.08.013>.
- Othman, M.R., Helwani, Z., Martunus, Fernando, W.J.N., 2009. Synthetic hydrotalcites from different routes and their application as catalysts and gas adsorbents: A review. *Appl. Organomet. Chem.* 23 (9), 335–346. <https://doi.org/10.1002/aoc.1517>.
- Pagadala, R., Maddila, S., Dasireddy, V.D.B.C., Jonnalagadda, S.B., 2014. Zn-VCO<sub>3</sub> hydrotalcite: A highly efficient and reusable heterogeneous catalyst for the Hantzsch dihydropyridine reaction. *Catal. Commun.* 45, 148–152. <https://doi.org/10.1016/j.catcom.2013.11.012>.
- Pratap, A.P., 2022. Greener Synthesis of Jasminaldehyde via Cross Aldol Condensation Reaction Using Recyclable Phase Transfer Catalysis and its Cosmetic Application. *Letters in Applied NanoBioScience* 12 (4), 104. <https://doi.org/10.33263/lianbs124.104>.
- Prentice, D.P., Gomez-Zamorano, L., Balonis, M., Erdemli, B., Ellison, K., Neithalath, N., Simonetti, D., Sant, G., 2020. The effects of (di-, tri-valent)-cation partitioning and intercalant anion-type on the solubility of hydrotalcites. *J. Am. Ceram. Soc.* 103 (10), 6025–6039. <https://doi.org/10.1111/jace.17324>.
- Rana, K.K., Rana, S., 2014. Microwave Reactors: A Brief Review on Its Fundamental Aspects and Applications. *OALib* 01 (06), 1–20. <https://doi.org/10.4236/oalib.1100686>.
- Rouquerol, J., Rouquerol, F., Grillet, Y., Denoyel, R., 1989. The role of thermal analysis and calorimetry in the study of porous or divided materials. *Thermochim Acta* 148 (C), 183–190. [https://doi.org/10.1016/0040-6031\(89\)85214-1](https://doi.org/10.1016/0040-6031(89)85214-1).
- Sahu, P.K., Sahu, P.K., Gupta, S.K., Agarwal, D.D., 2013. Role of calcinations and basicity of hydrotalcite as catalyst for environmental benign novel synthesis of 4H-pyrimido[2,1-b][1,3]benzothiazole derivatives of curcumin. *Cat. Sci. Technol.* 3 (6), 1520–1530. <https://doi.org/10.1039/c3cy20807a>.
- Serhan, M., Sprowls, M., Jackemeyer, D., Long, M., Perez, I. D., Maret, W., Tao, N., & Forzani, E. (2019). Total iron measurement in human serum with a smartphone. *AIChE Annual Meeting, Conference Proceedings, 2019-Novem.* <https://doi.org/10.1039/x0xx00000x>.
- Sharma, S.K., Patel, H.A., Jasra, R.V., 2008. Synthesis of jasminaldehyde using magnesium organo silicate as a solid base catalyst. *J. Mol. Catal. A Chem.* 280 (1–2), 61–67. <https://doi.org/10.1016/j.molcata.2007.10.013>.
- Sharma, S.K., Parikh, P.A., Jasra, R.V., 2010. Applied Catalysis A : General Reconstructed Mg / Al hydrotalcite as a solid base catalyst for synthesis of jasminaldehyde. “Applied Catalysis A, General” 386 (1–2), 34–42. <https://doi.org/10.1016/j.apcata.2010.07.021>.
- Sudheesh, N., Sharma, S.K., Khokhar, M.D., Shukla, R.S., 2011. Kinetic investigations on the modified chitosan catalyzed solvent-free synthesis of jasminaldehyde. *J. Mol. Catal. A Chem.* 339 (1–2), 86–91. <https://doi.org/10.1016/j.molcata.2011.02.016>.
- Tampieri, A., Lilic, M., Constanti, M., Medina, F., 2020. Microwave-assisted aldol condensation of furfural and acetone over Mg–Al hydrotalcite-based catalysts. *Crystals* 10 (9), 1–13. <https://doi.org/10.3390/cryst10090833>.
- Varma, R.S., 2001. Solvent-free accelerated organic syntheses using microwaves. *Pure Appl. Chem.* 73 (1), 193–198. <https://doi.org/10.1351/pac200173010193>.
- Wang, Q., Ohare, D., 2012. Recent advances in the synthesis and application of layered double hydroxide (LDH) nanosheets. *Chem. Rev.* 112 (7), 4124–4155. <https://doi.org/10.1021/cr200434v>.
- Wong, S.F., Deekamwong, K., Wittakayun, J., Ling, T.C., Muzara, O., Lee, H.L., Adam, F., Ng, E.P., 2018. Nanocrystalline K-F zeolite from rice husk silica as an eco-friendly solid base catalyst for the synthesis of jasminaldehyde under microwave irradiation. *Sains Malaysiana* 47 (2), 337–345. <https://doi.org/10.17576/jsm-2018-4702-16>.
- Zhang, C.Y., Shao, W.L., Zhou, W.X., Liu, Y., Han, Y.Y., Zheng, Y., Liu, Y.J., 2019. Biodiesel production by esterification reaction on k<sup>+</sup> modified mgal-hydrotalcites catalysts. *Catalysts* 9 (9). <https://doi.org/10.3390/catal9090742>.
- Zhang, Y., Xue, C., Xue, Y., Gao, R., Zhang, X., 2005. Determination of the degree of deacetylation of chitin and chitosan by X-ray powder diffraction. *Carbohydr. Res.* 340 (11), 1914–1917. <https://doi.org/10.1016/j.carres.2005.05.005>.
- Zheng, L., Bing, W., Wang, H., Zheng, L., Rao, D., Yang, Y., Wang, B., Wang, Y., Wei, M., 2018. A CaMnAl-hydrotalcite solid basic catalyst toward the aldol condensation reaction with a comparable level to liquid alkali catalysts. *Green Chem.* 20 (13), 3071–3080. <https://doi.org/10.1039/c8gc00851e>.